Dimensionless numbers in additive manufacturing

T. Mukherjee, V. Manvatkar, A. De, and T. DebRoy

Citation: J. Appl. Phys. **121**, 064904 (2017); doi: 10.1063/1.4976006
View online: http://dx.doi.org/10.1063/1.4976006
View Table of Contents: http://aip.scitation.org/toc/jap/121/6
Published by the American Institute of Physics

Dimensionless numbers in additive manufacturing

T. Mukherjee, V. Manvatkar, A. De, and T. DebRoy[a)]
Department of Materials Science and Engineering, The Pennsylvania State University, University Park, Pennsylvania 16802, USA

(Received 14 November 2016; accepted 28 January 2017; published online 13 February 2017)

The effects of many process variables and alloy properties on the structure and properties of additively manufactured parts are examined using four dimensionless numbers. The structure and properties of components made from 316 Stainless steel, Ti-6Al-4V, and Inconel 718 powders for various dimensionless heat inputs, Peclet numbers, Marangoni numbers, and Fourier numbers are studied. Temperature fields, cooling rates, solidification parameters, lack of fusion defects, and thermal strains are examined using a well-tested three-dimensional transient heat transfer and fluid flow model. The results show that lack of fusion defects in the fabricated parts can be minimized by strengthening interlayer bonding using high values of dimensionless heat input. The formation of harmful intermetallics such as laves phases in Inconel 718 can be suppressed using low heat input that results in a small molten pool, a steep temperature gradient, and a fast cooling rate. Improved interlayer bonding can be achieved at high Marangoni numbers, which results in vigorous circulation of liquid metal, larger pool dimensions, and greater depth of penetration. A high Fourier number ensures rapid cooling, low thermal distortion, and a high ratio of temperature gradient to the solidification growth rate with a greater tendency of plane front solidification. *Published by AIP Publishing*. [http://dx.doi.org/10.1063/1.4976006]

I. INTRODUCTION

The microstructure and properties of components made by additive manufacturing (AM) vary widely depending on the process parameters selected. These variations originate from the differences in the heat and mass transfer, fluid flow, and solidification during AM, which are influenced by a large number of variables.[1–5] In the laser assisted AM, the variables include laser power, scanning speed, power density, powder flow rate, gas flow conditions, beam traverse path, hatch spacing, layer thickness, and many thermo-physical properties including thermal conductivity, specific heat, density, and solidus and liquidus temperatures of the alloy.[6–9] Achieving structurally sound and reliable components by AM involves understanding and controlling many process variables individually and in appropriate combinations.

There are three main reasons why groups of variables rather than individual variables are of interest in understanding the evolution of the structure and properties of the components made by AM. First, it reduces the number of parameters that need to be investigated in a multi-variable and complex system such as AM. Second, when a group of variables are combined in a non-dimensional form with important physical meanings, such groups of variables, and not the individual constituent variables, express the behavior of the system such as AM. Third, important insights can be totally missed when systematic experiments are conducted by varying one individual variable at a time because such results rarely provide any clue about the influence of the interdependence of a group of variables on the structure and properties of the components.

There are four groups of non-dimensional variables that are of specific interest in AM. First, the non-dimensional heat input represents the ratio of the laser power to scanning speed and is responsible for cooling rates, solidification parameters, fusion zone shape and size, and several other important effects. Second, the Peclet number (Pe) indicates the relative importance of convection and conduction in heat transfer within the melt pool and determines the very mechanism by which the heat is transported within the fusion zone. Third, the Marangoni number (Ma) depicts the magnitude of surface tension force relative to viscous force in the melt pool and is a measure of the strength of the convective transport of heat. By influencing the magnitudes of liquid metal velocities within the melt pool, it affects the geometry of the pool, which is responsible for the solidification structure, thermal distortion, microstructure, and mechanical properties. Finally, the Fourier number (Fo) is the ratio of the rate of diffusive heat transport to the rate of heat storage and critical in understanding the damage heat can do to the components produced by AM. Taken as a whole, these four non-dimensional parameters affect the structure and properties of components built by AM like no individual AM variable.

Because AM is an emerging field, the influential literature in the field is growing, but there is already unmistakable proof about the influence of the four aforementioned non-dimensional numbers in welding and casting. Wei *et al.*[10] showed that in conduction mode laser welding, the Peclet number, Marangoni number, and dimensionless heat input control the shape of the fusion boundary, which in turn affects the solidification process, microstructure, and properties of the weld. Lu *et al.*[11] utilized both the Marangoni number and the Peclet number to explain the variation of the weld pool aspect ratio with respect to heat input and

[a)]Author to whom correspondence should be addressed. Electronic mail: debroy@psu.edu

shielding gas type for gas tungsten arc welding (GTAW) of stainless steel. Robert and DebRoy[12] showed that the unusual shapes of the fusion zone could be correlated using Pe and Ma in laser spot welding. Wei *et al.*[13] explained the difference in the weld pool shape based on the magnitude of the Marangoni number. Weckman *et al.*[14] showed that higher values of Fo slowed down the growth of the melt pool in pulsed laser welding of AISI 409 and AA 1100. Mukherjee *et al.*[15] presented correlations between the thermal strain and Fourier number for the AM of several alloys. Elsen *et al.*[16] and Mazumder[17] used a set of non-dimensional variables to explain the collective influence of process parameters and material behavior during laser processing. The non-dimensional variables correlated processing conditions and alloy properties with heat transfer and fluid flow phenomena and their influence on the structure and properties of the AM components.

Here, we investigate the roles of four well-established dimensionless numbers,[16] non-dimensional heat input, Peclet number, Marangoni number, and Fourier number in the laser based directed energy deposition of three widely used alloys, SS 316, IN 718, and Ti-6Al-4V. A well-tested, three dimensional, transient model is used to compute heat transfer and fluid flow in laser assisted AM. The computed results are examined to understand the role of non-dimensional parameters on the geometry of the fusion zone, solidification parameters, cooling rates, thermal distortion, and other attributes of the AM parts. Although the results presented here are for the laser based directed energy deposition AM process, this approach can be useful for understanding other AM processes.

II. NON-DIMENSIONAL NUMBERS AND THEIR CALCULATIONS

Heat input, which is the ratio of laser power to scanning speed, profoundly affects the structure and properties of the components in both meso and micro-scales. Macro-porosity (pores of equivalent diameters greater than 10 μm), morphology of the solidification front, scale of microstructures, phase compositions, and mechanical properties are affected by heat input like no other variable in 3D printing because they significantly affect temperature fields, thermal cycles, and solidification parameters. A non-dimensional heat input (Q^*) is considered as

$$Q^* = (P/V)/(P_R/V_R), \tag{1}$$

where P and V refer to the laser power and the scanning speed, respectively. P_R and V_R represent the reference laser power and scanning speed that provide the lowest heat input per unit length among the range of process parameters. The non-dimensional heat input, Q^*, therefore provides a measure of the energy deposited per unit length of the deposit.

The convective heat flow inside the molten pool controls the local cooling rate, the G/R ratio, and the solidification process. The relative importance of heat transfer by convection and conduction can be determined from the Peclet number[16]

$$Pe = \frac{UL}{\alpha}, \tag{2}$$

where U is the characteristic velocity, α is the thermal diffusivity of the alloy, and L is the characteristic length. The velocities at the molten pool surface are higher than those in the interior of the pool. The maximum velocity of the molten metal is considered as the characteristic velocity to calculate Pe. The characteristic length in Eq. (2) is considered as the length of the molten pool. A high value of the Peclet number indicates that convective heat transfer is the main mechanism of heat transfer within the liquid metal pool.

The shape and size of the build and the aspect ratio of the molten pool depend on the flow of liquid metal driven primarily by the spatial variation of interfacial tension, also known as the Marangoni stress. Effects of the Marangoni stress on the molten metal velocity is quantified by the Marangoni number[16]

$$Ma = -\frac{d\gamma}{dT}\frac{w\Delta T}{\mu\alpha}, \tag{3}$$

where μ is the dynamic viscosity, α is the thermal diffusivity of the alloy, w is the characteristic length of the molten pool, which is taken as the width of the molten pool, ΔT is the difference between the maximum temperature inside the pool and the solidus temperature of an alloy, and $\frac{d\gamma}{dT}$ is the sensitivity of surface tension gradient with respect to temperature (Table I). For most alloys that do not contain any surface active elements, this quantity is negative.[18] Higher heat input

TABLE I. Thermo-physical properties of SS 316, Ti-6Al-4V, and IN 718.[3,24]

Properties	SS 316	Ti-6Al-4V	IN 718
Liquidus temperature (K)	1733	1928	1609
Solidus temperature (K)	1693	1878	1533
Thermal conductivity (W/m K)	$11.82 + 0.0106\ T$	$1.57 + 1.6 \times 10^{-2}\ T - 1 \times 10^{-6}\ T^2$	$0.56 + 2.9 \times 10^{-2}\ T - 7 \times 10^{-6}\ T^2$
Specific heat (J/kg K)	$330.9 + 0.563\ T - 4.015 \times 10^{-4}\ T^2 + 9.465 \times 10^{-8}\ T^3$	$492.4 + 0.025\ T - 4.18 \times 10^{-6}\ T^2$	$360.4 + 0.026\ T - 4 \times 10^{-6}\ T^2$
Density (kg/m^3)	7800	4000	8100
Volumetric expansion co-efficient (/K)	5.85×10^{-5}	2.5×10^{-5}	4.8×10^{-5}
Viscosity (kg/m s)	7×10^{-3}	4×10^{-3}	5×10^{-3}
$d\gamma/dT$ (N/m K)	-0.40×10^{-3}	-0.37×10^{-3}	-0.26×10^{-3}
Absorption coefficient in liquid (η_l)	0.3	0.3	0.3
Absorption coefficient in powder (η_P)	0.7	0.7	0.7

during AM increases both the peak temperature and the pool dimensions and results in larger values of *Ma*.

Residual stress and distortion are important considerations in AM since multiple cycles of heating, melting, and solidification take place over a prolonged time period. It is the portion of the laser energy that fails to dissipate rapidly and leads to accumulation of heat, large pool size, high thermal strain and distortion, and residual stresses. The Fourier number (F_o) is a relative measure of the heat dissipation rate to the heat storage rate[19]

$$F_o = \alpha\tau/L^2, \tag{4}$$

where α, τ, and L refer to thermal diffusivity, characteristic time scale, and length, respectively. The Fourier number is an inverse measure of how much heat is stored within the component in relation to heat dissipation, and therefore, a higher Fo is desirable. The characteristic time can be expressed as L/V, where L and V are the pool length and scanning speed, respectively. The length of the molten pool is calculated using the heat transfer and fluid flow model. So, Eq. (4) can be re-written as follows:

$$F_o = \alpha/VL. \tag{5}$$

Higher heat input results in a larger molten pool, higher peak temperature, and reduced temperature gradient. As a result, the heat dissipation from the molten pool slows down.

III. HEAT TRANSFER AND FLUID FLOW MODEL

A well tested, three dimensional, transient, heat transfer, and fluid flow model for AM[3,20] is used to compute temperature and liquid metal velocity fields. The model solves the following equations of conservation of mass, momentum, and energy[21,22] in three dimensions

$$\frac{\partial(\rho u_i)}{\partial x_i} = 0, \tag{6}$$

$$\frac{\partial(\rho u_j)}{\partial t} + \frac{\partial(\rho u_j u_i)}{\partial x_i} = \frac{\partial}{\partial x_i}\left(\mu\frac{\partial u_j}{\partial x_i}\right) + S_j, \tag{7}$$

where ρ is the density, u_i and u_j are the velocity components along the i and j directions, respectively, and x_i is the distance along the i direction, t is the time, μ is the dynamic viscosity, and S_j is a source term for the momentum equation. The energy conservation equation[8] is

$$\rho\frac{\partial h}{\partial t} + \frac{\partial(\rho u_i h)}{\partial x_i} = \frac{\partial}{\partial x_i}\left(\frac{k}{C_p}\frac{\partial h}{\partial x_i}\right) - \rho\frac{\partial\Delta H}{\partial t} - \rho\frac{\partial(u_i\Delta H)}{\partial x_i}, \tag{8}$$

where h is the sensible heat, C_p is the specific heat, k is the thermal conductivity, and ΔH is the latent heat content.

The simulations are carried out for the deposition of multilayer structures. The solution domain represents the substrate, deposited layers, and the surrounding gas. Calculations are done over half of the geometry taking advantage of symmetry in many small time steps. Transfer of laser beam energy to the system is defined through a volumetric heat source term. This heat source accounts for the laser energy transfer to powder while in flight from the powder nozzle to the substrate and also after the material reaches the substrate. The volumetric heat source is expressed by the following equation:[23]

$$S_i = \frac{Pd}{\pi r_b^2 t}[\eta_P + (1-\eta_P)\eta_l]\exp\left(-d\frac{r^2}{r_b^2}\right), \tag{9}$$

where η_p is the fraction of laser energy absorbed by the powder during flight from the nozzle to the substrate, P is the nominal laser power, d is the laser beam intensity distribution factor, t is the layer thickness, r_b is the focused beam radius, and r is the radial distance from the beam axis. The first term within the bracket accounts for laser beam energy transferred to the particles during their flight, and second term considers the energy absorbed by the growing layer due to irradiation of the laser beam on the depositing surface. The term η_l refers to the absorption coefficient of the growing layer. The absorption coefficients in Eq. (9) are provided in Table I. The boundary conditions for the thermal analysis include heat loss by convection and radiation with the surroundings. The velocities assigned at the top free surface as boundary conditions are estimated based on surface tension variation due to temperature gradient.

To ensure that there is no energy and mass transfer across the symmetry plane, the spatial gradients of temperature and velocities at the plane of symmetry are set to zero. The initial temperature of the solution domain is considered to be known. Analysis starts with the assignment of substrate properties to all grid points within the substrate. At all grids outside the substrate, the grids are assigned properties of the gas that surrounds the substrate, i.e., argon. For each small stepwise movement of the laser beam, properties of a set of cells under the beam are updated from gas properties to properties of the alloy at the local temperature. After a layer is deposited, an idle time is considered when the laser is switched off. The deposition of a new layer starts from the initial location above the previously deposited layer. The procedure is repeated until the simulation of all the layers is completed. Calculations are continued until the specimen cools to ambient temperature. Simultaneously, the boundary conditions and initial temperature of the solution domain are updated after every time step.

More details about the modeling of powder injection and the solution methodology for AM are described in our previous publications[3,20] and are not repeated here. Only the salient features are indicated here. A control volume method is implemented to discretize the governing equations by dividing the solution domain into small volumes. The discretized equations are solved iteratively using the tri-diagonal matrix algorithm.[3,20] The calculations are performed using an in-house Fortran code compiled using an Intel Fortran compiler. Non-uniform fixed grids are used in the solution domain with finer grid points within the layers and coarser ones in the substrate to achieve a good resolution of variable values and computational accuracy. A solution domain of 20 mm × 3.5 mm × 7.8 mm (length × width × height) is divided into 2,755,000

$(580 \times 50 \times 95)$ grid points. At each time-step, the iterative calculations are continued till the sum of accumulation and heat loss is almost equal to heat input with an imbalance of less than 0.5%, and also, the temperature and velocity components at all grid points satisfy the respective discretized equations within a pre-set error limit of $\pm 0.1\%$. Typically, a total of about 3.5×10^9 linear equations are solved cumulatively to obtain temperature and velocity components for all the time-steps along one layer that takes approximately 28 min in a personal computer with a 3.40 GHz i7 processor and 8 GB RAM.

IV. RESULTS AND DISCUSSION

A. Deposition of SS 316, Ti-6Al-4V, and IN 718 alloys

Figures 1(a)–1(c) show the computed melt pool geometry for the deposition of SS 316, Ti-6Al-4V, and IN 718 for a constant laser power and scanning speed. The red and green bands in the figures indicate the liquid and two phase solid-liquid regions, respectively. The arrows represent velocity vectors in the melt pool, and a reference vector is shown to indicate the magnitudes of the velocities in the melt pool. The bigger pool size for Ti-6Al-4V is attributed to its lower density and thermal diffusivity compared to that for the other two alloys. As expected, higher power results in larger pools for each of the alloys as observed from Figures 1(d)–1(f). The results clearly show that both the processing conditions and the thermo-physical properties of the alloy significantly influence the geometry of the melt pool.

Figure 2 shows a fair agreement between the numerically computed and the corresponding experimentally measured melt pool widths for various layers in a seven layer SS 316 component. Both the computed and the measured results show progressively larger melt pools as the deposition moves to upper layers. However, the increase in pool size is less pronounced in the upper layers. The heat loss from the melt pool to the substrate decreases as more layers are deposited. A slight over-estimation of the computed pool size in Figure 2 is attributed to the uncertainty in the actual rates of heat input and heat loss in the presence of a stream of alloy powder. The agreement between the computed and the experimental results indicates that the model can be used for the calculation of cooling rates, solidification parameters, and the non-dimensional numbers with confidence.

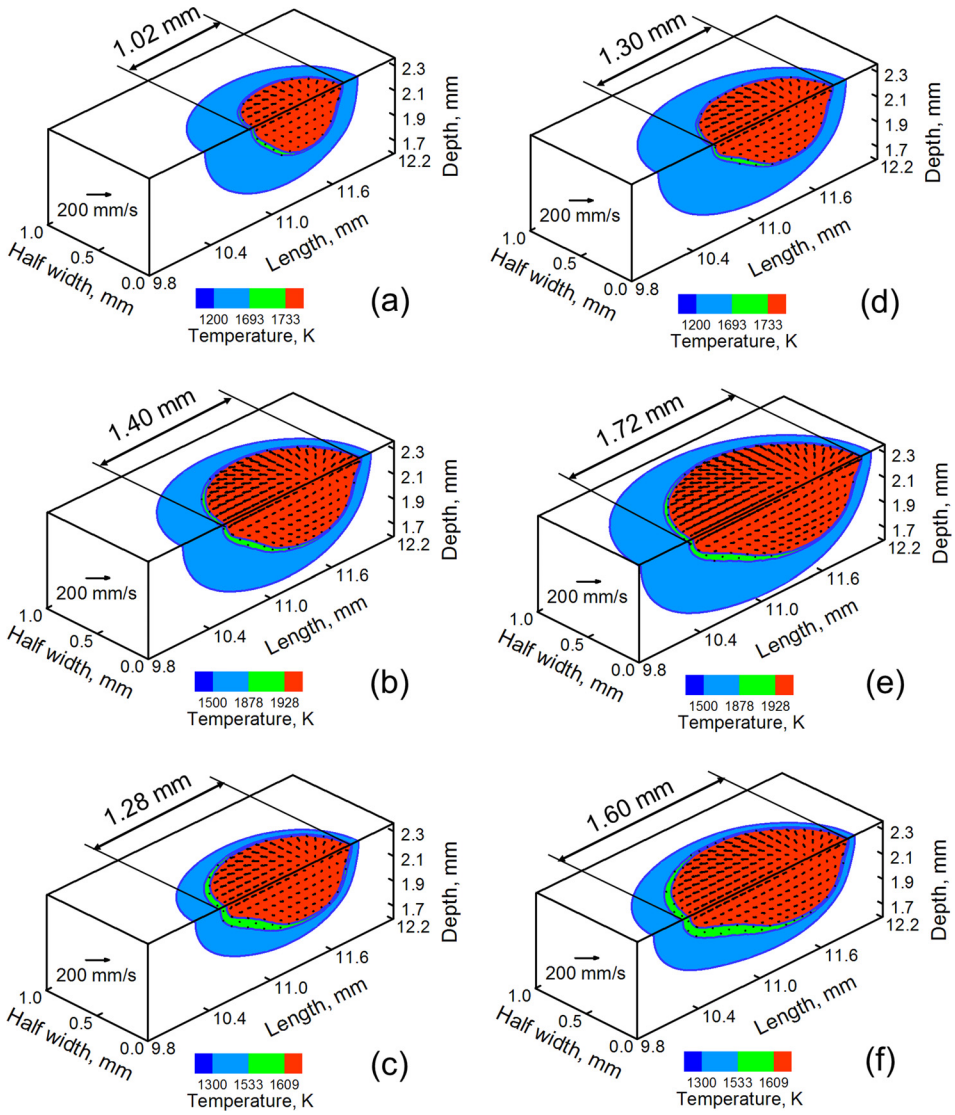

FIG. 1. Temperature and velocity field for a laser power of 190 W for (a) SS 316, (b) Ti-6Al-4V, and (c) IN 718 and of 230 W for (d) SS 316, (e) Ti-6Al-4V, and (f) IN 718. All data are for 15 mm/s scanning speed and at the mid length of the 5th layer.

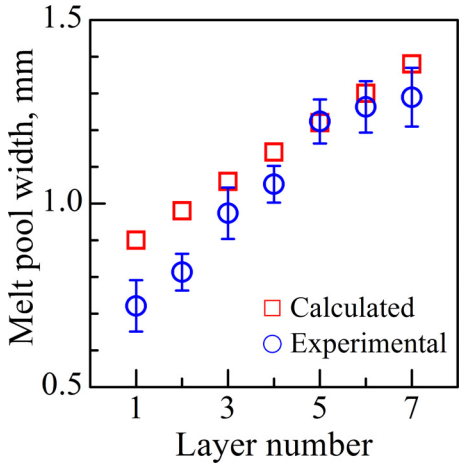

FIG. 2. Comparison of calculated and experimentally measured[25] pool widths for a 7 layer deposition of SS 316. The errors in the experimental measurements are estimated from several readings taken along the layer thickness.

B. Non-dimensional heat input

Figure 3 shows the variation of non-dimensional peak temperature, which is the ratio of the peak temperature, T_P, to the liquidus temperature, T_L, as a function of the non-dimensional heat input, Q^*. As anticipated, the ratio T_P/T_L increases with the increase in Q^* for all three alloys. The reference heat input for Eq. (1) is estimated considering 190 W laser power and 15 mm/s scanning speed, which results in the minimum heat input among the processing conditions listed in Table II. The same heat input is used for all subsequent calculations of non-dimensional heat input unless otherwise specified. Figure 4(a) shows the variations of computed melt pool length in non-dimensional form as a function of non-dimensional heat input Q^* for the three alloy powders. The computed melt pool lengths are the highest for Ti-6Al-4V, which is attributed to its lowest density. Alloys IN 718 and SS 316 have nearly the same density, but the lower liquidus temperature of the former results in greater melt pool size for the same heat input Q^*. Higher heat input can ensure larger melt pools to ensure adequate re-melting of the previously deposited layer to achieve good interlayer

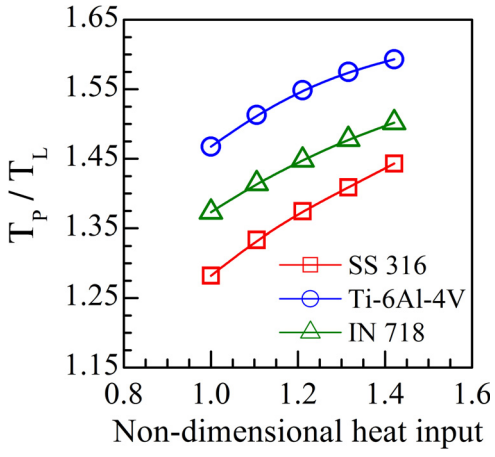

FIG. 3. Effects of the non-dimensional heat input on non-dimensional peak temperature for three alloys.

TABLE II. Process parameters used for calculations.

Laser power (W)	Beam radius (mm)	Scanning speed (mm/s)	Layer thickness (mm)	Substrate thickness (mm)	Powder flow rate (gm/s)
190–270	0.5	15	0.38	4	0.416

bonding. Lack of fusion between two successively deposited layers results in porosity,[9] which adversely affects mechanical properties.[9,15] The porosity due to the lack of fusion between two successively deposited layers can be minimized by increasing heat input. Figure 4(b) shows that the heat input can be correlated with the experimentally measured volume percentage of pores for five different alloys.[26–30] The reference heat input for Figure 4(b) is estimated considering the 175 W laser power and 70 mm/s scanning speed, which provide the minimum heat input among all the process parameter data obtained from the literature.[26–30]

The temperature gradient, G, and the solidification growth rate, R, provide useful information about the evolution of the solidification structure. In particular, GR gives the local cooling rate and G/R influences the morphology of the solidification front.[31,32] Figure 5(a) shows that the calculated cooling rate for a laser assisted AM of SS 316 agrees well with the experimental data.[33] However, errors in the cooling rate estimation are not available in the literature. The reduction of the cooling rate with the heat input (Q^*) is attributed to slower cooling of larger melt pools for high values of Q^*. The variations of the cooling rates are also shown in Figures 5(b) as a function of Q^* for the three alloys. The cooling rates are calculated between the liquidus and solidus temperatures of the alloys at a height of 3.8 mm from the substrate in the mid point of a 20 mm long track. The Ti-6Al-4V deposit attains a higher peak temperature than SS 316 because of its lower density. Ti-6Al-4V also cools slower than SS 316 because of its lower thermal conductivity. However, the slower cooling rate of IN 718 than that of SS 316 can be attributed to its larger pool volume.

For the laser assisted AM of SS 316, a columnar dendritic microstructure secondary arm spacing, d, in the range of 3–10 μm is observed[3,25,34] depending on the cooling rate, CR. The interdependence between the two variables is given by[3]

$$d = A(CR)^{-n}, \tag{10}$$

where d is in μm, CR is the cooling rate in K/s, and A and n are material specific constants having values of 25 and 0.28, respectively.[35] Previous research studies[3,25,36] have shown that for a very fine columnar dendritic structure, the yield strength (σ_y) can be correlated with the secondary dendritic arm spacing[3]

$$\sigma_y = \sigma_0 + K_y\,(d)^{-0.5}, \tag{11}$$

where σ_0 and K_y are constants whose values for SS 316[3] are 150 MPa and 575 MPa $(\mu m)^{0.5}$, respectively. The hardness is related to the yield strength[3]

$$H_v = 3\sigma_y\,(0.1)^{-0.25}. \tag{12}$$

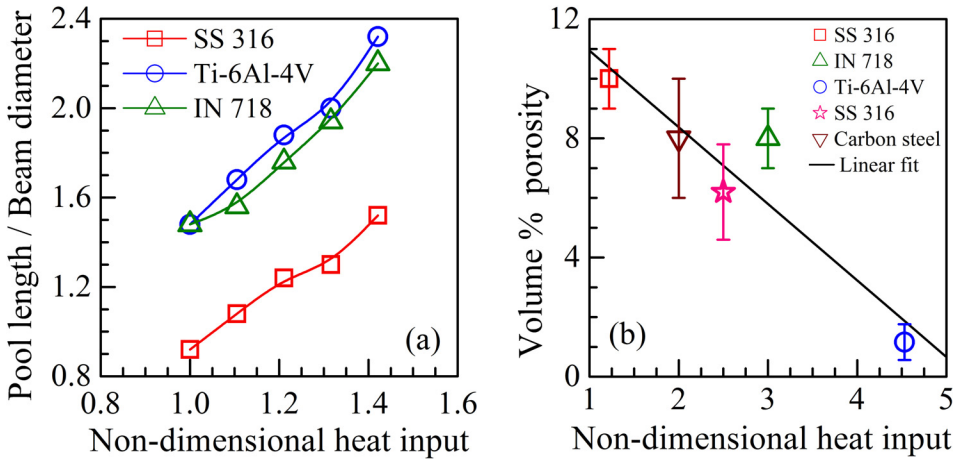

FIG. 4. Effects of the non-dimensional heat input on (a) non-dimensional pool length and (b) volume percentage of lack of fusion porosity for Ti-6Al-4V,[26] IN 718,[27] SS 316,[28] carbon steel,[29] and SS 316.[30] The errors shown are rough estimates based on the data provided in the literature.

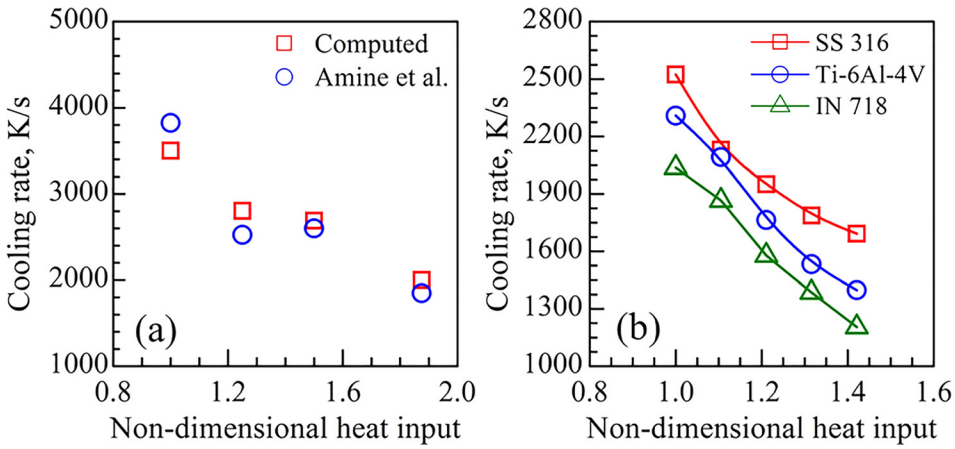

FIG. 5. Effects of the non-dimensional heat input on (a) the cooling rate validated using the data from the literature[33] and (b) the cooling rate for three alloys.

From Eqs. (10)–(12), it is clear that the smaller secondary dendrite arm spacing due to rapid cooling results in higher hardness. Therefore, low heat input results in harder deposits owing to faster cooling as shown in Figure 6(a). This figure also indicates that the calculated hardness for SS 316 agrees well with the experimental data. The presence of laves phases can be detrimental to the mechanical properties of the nickel base superalloys such as IN 718.[37] Formation of these intermetallic compounds can be suppressed by increasing the cooling rate. For example, Nie *et al.*[7] reported a decrease in the volume fraction of the laves phase from 16% to 4% due to an increase in the cooling rate from 500 K/s to 4000 K/s. Parimi *et al.*[38] reported that the parts having the laves phase of 20–30 μm size exhibited worse mechanical properties than that having 1–2 μm size. A rapid cooling due to low heat input can effectively reduce the size of the laves phase as shown in Figure 6(b). This figure is plotted by considering the data from different sources in the literature[38–41] on laser based AM of IN 718. The error values shown are roughly estimated based on the data reported in the literature.

The effect of heat input on the ratio G/R is shown in Figure 7. The temperature gradient in the melt pool is the smallest with IN 718 deposits followed by that in Ti-6Al-4V

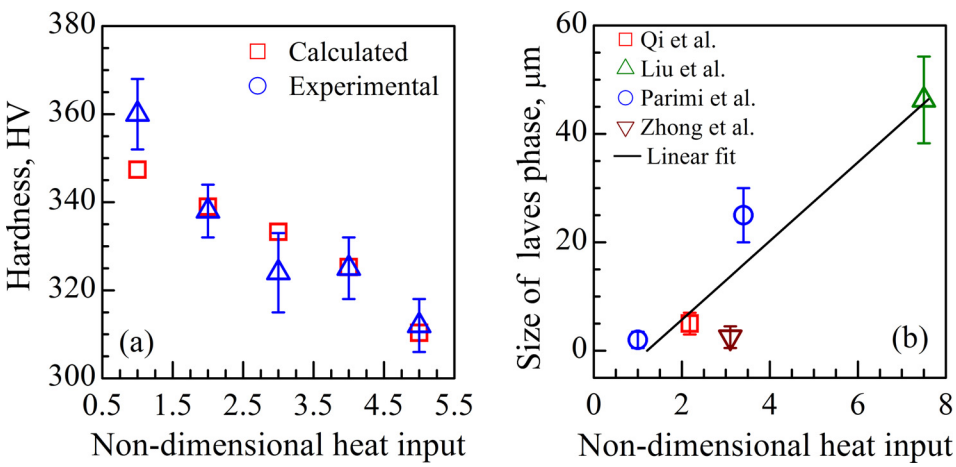

FIG. 6. Effects of the non-dimensional heat input on (a) Vicker's hardness validated using experimental data[35] and (b) size of the laves phase for laser assisted AM of IN 718.[38–41]

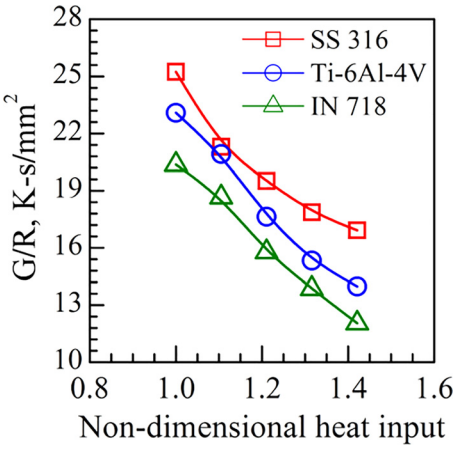

FIG. 7. Variation of the G/R ratio with respect to the heat input for three alloys.

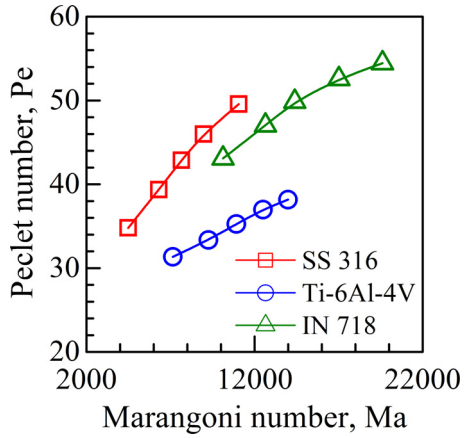

FIG. 9. Relation between the Peclet number and Marangoni number.

and SS 316 alloy deposits. As a result, the SS 316 deposits exhibit the highest G/R followed by that of Ti-6Al-4V and IN 718 alloy deposits.

C. Peclet and Marangoni numbers

Higher heat input increases both the pool length and the velocity of the liquid metal in the melt pool. Therefore, the Peclet number increases with heat input as shown in Figure 8(a) and its value is much higher than 10 for all the cases considered here. These high values indicate that convective heat transfer is the main mechanism of heat transfer within the melt pool. Of the three alloys, Ti-6Al-4V and IN 718 have the highest and the lowest values of thermal diffusivity, respectively (Table I). Therefore, the role of convective heat transfer is the most and the least pronounced for IN 718 and Ti-6Al-4V, respectively, as shown in Figure 8(a).

The Marangoni number, Ma, increases with heat input as shown in Figure 8(b). For a specific heat input, the molten pool volumes of both Ti-6Al-4V and IN 718 deposits are higher than that of SS 316. As a result, both Ti-6Al-4V and IN 718 exhibit higher Marangoni numbers than SS 316. Higher values of the Marangoni number indicate larger velocities of liquid metal in the molten pool. Figure 9 shows that an increase in the Marangoni number also results in higher values of the Peclet number and a more pronounced convective heat transfer within the molten pool.

Higher Ma indicates larger liquid metal velocity and more efficient convective heat transfer, which, in turn, results in a larger liquid metal pool. Lighter alloys also result in a larger molten pool since a smaller weight of alloys is contained in a given volume. Therefore, a combined effect of density and Ma is examined in Figure 10. Both the length and the aspect ratio of the melt pool are enhanced due to higher Ma and lower density of the alloy powder.

D. Fourier number

Susceptibility of alloys to thermomechanical damage (residual stress and distortion) is influenced by their ability to diffuse heat rapidly. The thermal diffusivity of Ti-6Al-4V is higher than those of the other two alloys, and it has the highest Fourier number because of its ability to diffuse heat most efficiently as shown in Figure 11(a). The figure also shows that the Fourier number decreases with an increase in heat input as anticipated. Both slow dissipation and high accumulation of heat result in a large molten pool. Large pools shrink more during solidification and exhibit pronounced thermal distortion. Therefore, a lower Fourier number enhances thermal distortion. In contrast, flexural rigidity of the substrate can resist thermal distortion in AM.[15] The flexural rigidity is defined as a product of elastic modulus, *E*,

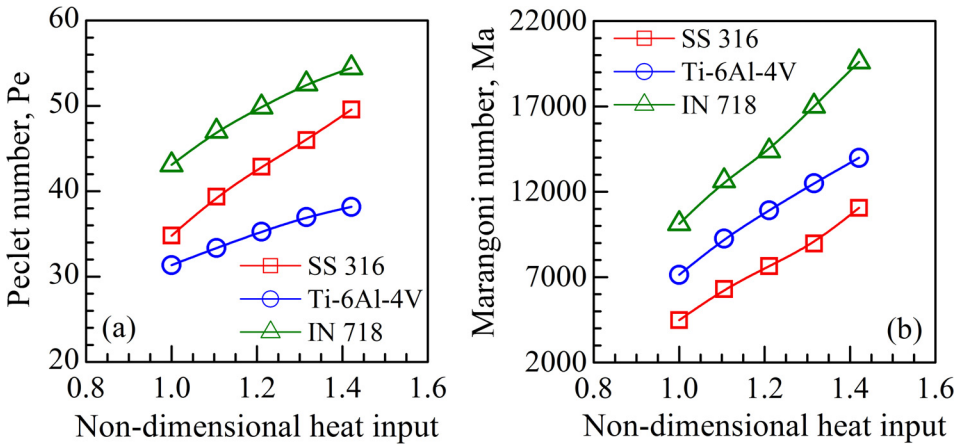

FIG. 8. Effect of linear heat input on the (a) Peclet number and (b) Marangoni number.

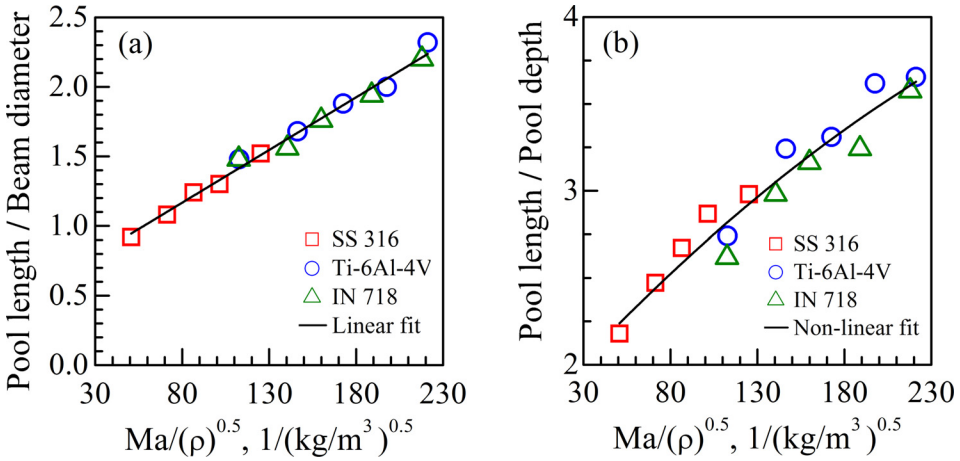

FIG. 10. Effects of the Marangoni number on (a) pool length and (b) aspect ratio of the pool.

of the alloy and the second moment of area, I, of the cross-section of the part geometry. It is recently shown that the following thermal strain parameter, ε^*, is directly related to distortion during solidification of alloys[15,19]

$$\varepsilon* = \frac{\beta \Delta T}{EI} \frac{t H^{3/2}}{F_o \sqrt{\rho}}, \tag{13}$$

where β is the volumetric coefficient of thermal expansion, ΔT is the maximum rise in temperature during the process, E is the elastic modulus, and I is the moment of inertia of the substrate, the product, EI, is the flexural rigidity of the structure, t is the characteristic time, H is the heat input per unit length, F_o is the Fourier number, and ρ is the density of the alloy powder. Figure 11(b) shows the combined effect of both the Fourier number and the flexural rigidity on the thermal strain parameter.[15] It is evident from Figure 11(b) that maintaining a high Fourier number by lowering the heat input is always an effective way to minimize thermal distortion during AM. Figure 11(c) also supports this fact for welding, which is similar to AM for the deposition of a single layer. This figure shows a direct correlation between thermal strain and heat input for three common alloys based on independent experimental data.[42,43] Therefore, a high Fo signifies rapid heat dissipation and low heat storage is desirable to mitigate the thermo-mechanical damage of the fabricated part.

Cooling rates between the liquidus and solidus temperatures of all alloys can be directly correlated with Fo as shown in Figure 12(a). Lower heat accumulation in smaller molten

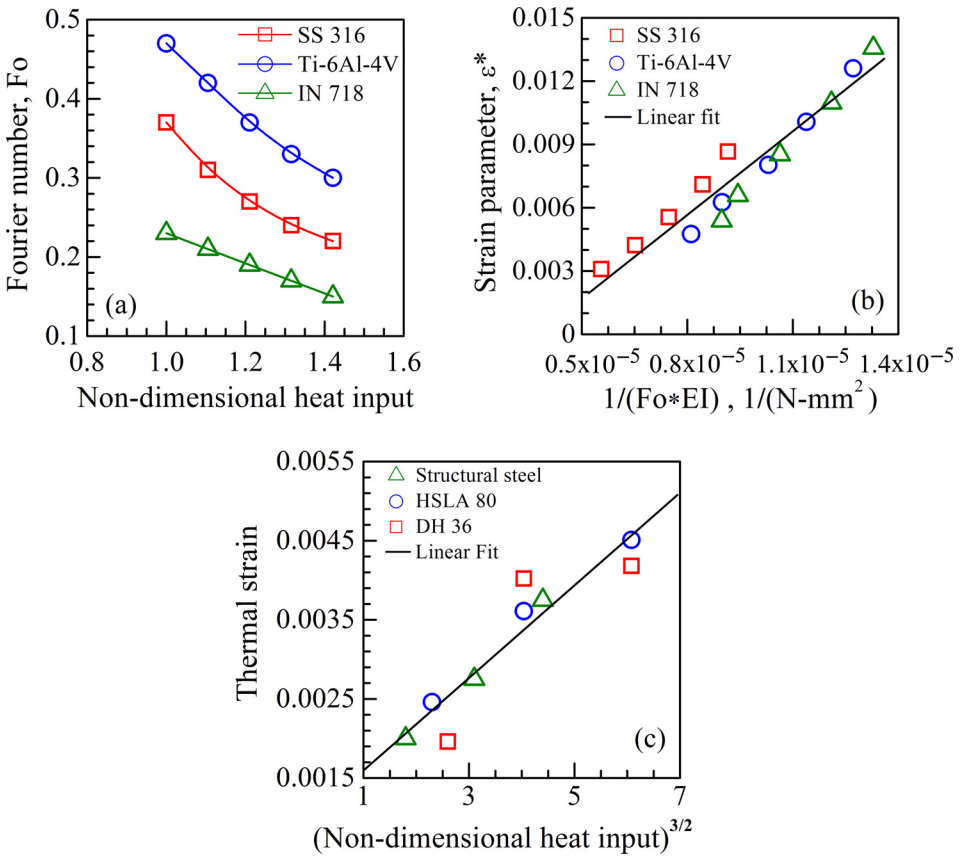

FIG. 11. (a) Fourier number as functions of linear heat input for three alloys, (b) effect of the Fourier number on the thermal strain parameter, and (c) effect of heat input on the thermal strain for structural steel,[42] tool steel,[43] and high strength low alloys steel[43] in welding.

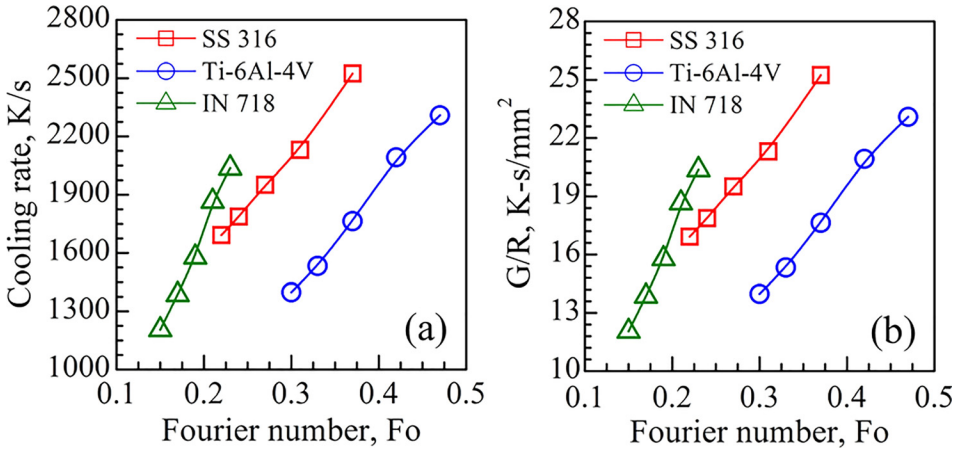

FIG. 12. Effect of the Fourier number on the (a) cooling rate and (b) G/R ratio.

pools results in a higher temperature gradient. Furthermore, a large Fourier number enhances the ratio of temperature gradient (G) to the solidification growth rate (R). Figure 12(b) indicates that the G/R ratio increases with the Fourier number for all alloys. The solid-liquid interface morphology tends to change from cellular, cellular-dendritic to equiaxed dendritic as the value of G/R decreases with a decrease in the Fourier number.

V. SUMMARY AND CONCLUSIONS

The role of non-dimensional numbers in the laser assisted AM of three commonly used engineering alloys, stainless steel 316, Ti-6Al-4V, and a nickel base super alloy IN 718, is examined using a well-tested 3D transient heat transfer and fluid flow model. In particular, the roles of a dimensionless heat input variable, Peclet number, Marangoni number, and Fourier number on temperature and velocity distribution, cooling rate, solidification parameters, hardness, amount of porosity, size of intermetallic compounds, and thermal distortion are evaluated. Below are the specific findings.

1. Higher heat input enhances the peak temperature and pool dimensions. The large pools ensure a stronger interlayer bonding that minimizes the porosity in the fabricated parts.
2. Cooling rates are enhanced for low heat inputs. Formation of the laves phases that are detrimental to the mechanical properties can be suppressed by enhancing the cooling rate in typical AM processing of IN 718 alloy powder.
3. For the conditions of laser assisted AM investigated in this paper, the Peclet numbers are greater than 10. These high values of Pe indicate that convective heat transfer is the main mechanism of heat transfer within the liquid metal pool.
4. A high Marangoni number indicates large velocities inside the molten pool. The rapid movement of the liquid metal inside the pool increases the pool dimensions and aspect ratio. Larger pools with a high aspect ratio promote sound inter layer bonding. Therefore, a high Marangoni number can reduce porosities formed by lack of fusion defects. However, very high Marangoni number may promote instability of the molten pool and increase the susceptibility to defect formation.
5. A high Fourier number can provide a rapid cooling rate and a high G/R ratio. An increase in the Fourier number can also reduce the thermal distortion during AM.

ACKNOWLEDGMENTS

We acknowledge the support from the U.S. Department of Energy NEUP under Grant No. DE-NE0008280. T.M. acknowledges the support from the American Welding Society research fellowship under Grant No. 179466.

[1]D. D. Gu, W. Meiners, K. Wissenbach, and R. Poprawe, Int. Mater. Rev. **57**, 133 (2012).
[2]T. DebRoy, W. Zhang, J. Turner, and S. S. Babu, Building digital twins of 3D printing machines, Scr. Mater. (2017).
[3]V. Manvatkar, A. De, and T. DebRoy, J. Appl. Phys. **116**, 1249051 (2014).
[4]H. Qi, J. Mazumder, and H. Ki, J. Appl. Phys. **100**, 024903 (2006).
[5]X. He and J. Mazumder, J. Appl. Phys. **101**, 053113 (2007).
[6]D. D. Gu and P. Yuan, J. Appl. Phys. **118**, 233109 (2015).
[7]P. Nie, O. A. Ojo, and Z. Li, Acta Mater. **77**, 85 (2014).
[8]A. Raghavan, H. L. Wei, T. A. Palmer, and T. DebRoy, J. Laser Appl. **25**, 052006 (2013).
[9]I. Gibson, D. Rosen, and B. Stucker, *Additive Manufacturing Technologies: 3D Printing, Rapid Prototyping and Direct Digital Manufacturing Ch.10* (Springer, New York, 2015).
[10]P. S. Wei, C. N. Ting, J. S. Yeh, T. DebRoy, F. K. Chung, and G. H. Yan, J Appl. Phys. **105**, 053508 (2009).
[11]S. Lu, H. Fujii, and K. Nogi, Scr. Mater. **51**, 271 (2004).
[12]A. Robert and T. DebRoy, Metall. Mater. Trans. B **32**, 941 (2001).
[13]P. S. Wei, J. S. Yeh, C. N. Ting, T. DebRoy, F. K. Chung, and C. L. Lin, Int. J Heat Mass Transfer **52**, 3790 (2009).
[14]D. C. Weckman, H. W. Kerr, and J. T. Liu, Metall. Mater. Trans. B **28**, 687 (1997).
[15]T. Mukherjee, J. S. Zuback, A. De, and T. DebRoy, Sci. Rep. **6**, 19717 (2016).
[16]M. Elsen, F. Al-Bender, and J.-P. Kruth, Rapid Prototyping J. **14**, 15 (2008).
[17]J. Mazumder, Opt. Eng. **30**, 1208 (1991).
[18]P. Sahoo, T. DebRoy, and M. J. McNallan, Metall. Trans. B **19**, 483 (1988).
[19]T. Mukherjee, V. Manvatkar, A. De, and T. DebRoy, Scr. Mater. **127**, 79 (2017).
[20]V. Manvatkar, A. De, and T. DebRoy, Mater. Sci. Technol. **31**, 924 (2015).
[21]S. A. David and T. DebRoy, Science **257**, 497 (1992).
[22]T. DebRoy and S. A. David, Rev. Mod. Phys. **67**, 85 (1995).
[23]T. Mukherjee, W. Zhang, and T. DebRoy, Comput. Mater. Sci. **126**, 360 (2017).
[24]K. C. Mills, *Recommended Values of Thermophysical Properties for Selected Commercial Alloys* (Cambridge, England, 2002).
[25]V. D. Manvatkar, A. A. Gokhale, G. J. Reddy, A. Venkataramana, and A. De, Metall. Mater. Trans. A **42**, 4080 (2011).

[26]C. J. Kong, C. J. Tuck, I. A. Ashcroft, R. D. Wildman, and R. Hague, in *Proceedings of the Solid Freeform Fabrication Symposium*, Austin, Texas, USA (2011), p. 475.
[27]Q. Jia and D. D. Gu, J. Alloys Compd. **585**, 713 (2014).
[28]A. B. Spierings, M. Schneider, and R. Eggenberger, Rapid Prototyping J. **17**, 380 (2011).
[29]M. A. Taha, A. F. Yousef, K. A. Gany, and H. A. Sabour, Materialwissenschaft und Werkstofftechnik **43**, 913 (2012).
[30]A. Mertens, S. Reginster, Q. Contrepois, T. Dormal, O. Lemaire, and J. Lecomte-Beckers, Int. Mater. Sci. Forum **783–786**, 898 (2014).
[31]H. L. Wei, J. Mazumder, and T. DebRoy, Sci. Rep. **5**, 16446 (2015).
[32]H. L. Wei, J. W. Elmer, and T. DebRoy, Acta Mater. **115**, 123 (2016).
[33]T. Amine, J. W. Newkirk, and F. Liou, Appl. Therm. Eng. **73**, 500 (2014).
[34]B. Zheng, Y. Zhou, J. E. Smugeresky, J. M. Schoenung, and E. J. Lavernia, Metall. Mater. Trans. A **39**, 2228 (2008).
[35]K. Zhang, S. Wang, W. Liu, and X. Shang, Mater. Des. **55**, 104 (2014).
[36]Z. Guo, N. Saunders, P. Miodownik, and J. P. Schillé, in *Proceedings of the ICAA11* (2008), Vol. 22, p. 26.
[37]G. D. Janaki Ram, A. V. Reddy, K. P. Rao, and G. M. Reddy, Sci. Technol. Weld. Joining **9**, 390 (2004).
[38]L. L. Parimi, G. A. Ravi, D. Clark, and M. M. Attallah, Mater. Charact. **89**, 102 (2014).
[39]H. Qi, M. Azer, and A. Ritter, Metal. Mater. Trans. A **40**, 2410 (2009).
[40]F. Liu, X. Lin, H. Leng, J. Cao, Q. Liu, C. Huang, and W. Huang, Opt. Laser Technol. **45**, 330 (2013).
[41]C. Zhong, A. Gasser, J. Kittel, J. Fu, Y. Ding, and R. Poprawe, J. Laser Appl. **28**, 022010 (2016).
[42]S. Okano, M. Mochizuki, M. Toyoda, and T. Ueyama, Sci. Technol. Weld. Joining **17**, 264 (2012).
[43]Y. P. Yang, R. Dull, H. Castner, T. D. Huang, and D. Fanguy, Weld. J. **93**, 421s (2014).